Magnetic Field Optimization of U-type Ironless Permanent Magnet Linear Motor Using Magnetic Permeable Block

Shuheng Qiu
Institute of Advanced Manufacturing Technology
Ningbo Institute of Materials Technology and Engineering, Chinese Academy of Sciences
Ningbo, China
qiushuheng@nimte.ac.cn

Jie Zhang
Institute of Advanced Manufacturing Technology
Ningbo Institute of Materials Technology and Engineering, Chinese Academy of Sciences
Ningbo, China
zhangjie@nimte.ac.cn

Xianbei Sun
Institute of Advanced Manufacturing Technology
Ningbo Institute of Materials Technology and Engineering, Chinese Academy of Sciences
Ningbo, China
sunxianbei@nimte.ac.cn

Chi Zhang*
Institute of Advanced Manufacturing Technology
Ningbo Institute of Materials Technology and Engineering, Chinese Academy of Sciences
Ningbo, China
zhangchi@nimte.ac.cn

Yunpeng Gao
Institute of Advanced Manufacturing Technology
Ningbo Institute of Materials Technology and Engineering, Chinese Academy of Sciences
Ningbo, China
gaoyunpeng@nimte.ac.cn

Rong Li
Institute of Advanced Manufacturing Technology
Ningbo Institute of Materials Technology and Engineering, Chinese Academy of Sciences
Ningbo, China
lirong@nimte.ac.cn

2021 13th International Symposium on Linear Drives for Industry Applications (LDIA) | 978-1-7281-7210-1/21/$31.00 ©2021 IEEE | DOI: 10.1109/LDIA49489.2021.9505791

***Abstract*—U-type ironless permanent magnet linear motors (IL-PMLMs) are widely used in high-performance applications due to the advantages of high speed, acceleration, precision, and low wear. The magnetic field in the back iron of the traditional U-shaped IL-PMLMs appears a strong and weak alternating phenomenon. And the peak magnetic density is too high, which raises the risk of saturation. By employing a magnetic permeable block at the end of IL-PMLMs, the homogeneity of the back iron magnetic field can be optimized. Also, the design method of the best size of the magnetic permeable block is proposed. Finally, the optimization results of the magnetic field are verified by the finite element model.**

Keywords—IL-PMLM, Magnetic permeable block, Back iron magnetic field, saturation.

I. INTRODUCTION

In modern industrial systems, permanent magnet linear motors (PMLMs) are widely used in reciprocating servo units, feed units, and conveying units due to their high power density, high system efficiency, and high positioning accuracy[1-3]. According to the presence or absence of the armature core, PMLMs can be divided into two types: iron-cored PMLMs and ironless PMLMs. Iron-cored PMLMs can produce greater thrust. However, due to the cogging and end effect, the thrust ripple of iron-cored PMLMs is also greater[4]. The ironless permanent magnet linear motor has the advantages of smaller thrust ripple, a more linear relationship between thrust and current, and weaker armature reaction[5]. Therefore, ironless PMLMs are widely used in high-precision applications. Among them, U-type ironless PMLMs shown in Fig.1 are the most widely used. Due to the lighter weight of the U-type PMLM mover, it also has higher performance on dynamic response.

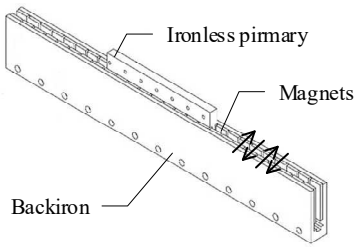

Fig.1 The basic structure of U-type Ironless PMLMs

The increase of the air gap magnetic flux density (MFD) can effectively increase the thrust density of the U-type PMLM. Sun Peng, et al. use a multi-objective function to optimize the magnet consumption to reduce the weight [6]. Liyi Li, et al. conducted electromagnetic-thermal coupling analysis for U-type PMLMs with Halbach magnet arrays, by which they optimized a set of high thrust density dimensional parameters[5]. Qiu Shuheng, et al compare the thrust characteristics of the U-type PMLMs employing Halbach/non-Halbach magnet arrays and stacked/non-stacked windings[7]. Lu Zhang et al. propose a novel double side Halbach permanent magnet array to gain a larger air gap magnetic flux density[8]. Li Zheng et al. use the layered model to analyze the air gap magnetic field of the U-type IL-PMLMs[9].

However, none of the above researches are paying attention to the magnetic field distribution in the back iron of U-type PMLMs. Through the FEA simulation of the full model of the U-type PMLM, it can be found that the flux generated by the magnets at the ends will all merge into the inner adjacent magnets to form a closed magnetic circuit, which is shown in Fig.2 (a). As a result, every two pieces of magnets form a complete and independent magnetic circuit, which generates alternating strong and weak magnetic fields in the back iron. Quantitatively, it can be found that the highest magnetic density in the back iron can reach 2.0T as

This paper is supported in part by Ningbo "Technology Innovation 2025" Major Project under grant 2018B10058 and 2018B10009, in part by Ningbo Key Core Technology Emergency Tackling Plan Project under grant 2020G001, in part by Natural Science Foundation of Zhejiang Province under grant LD21E070002。

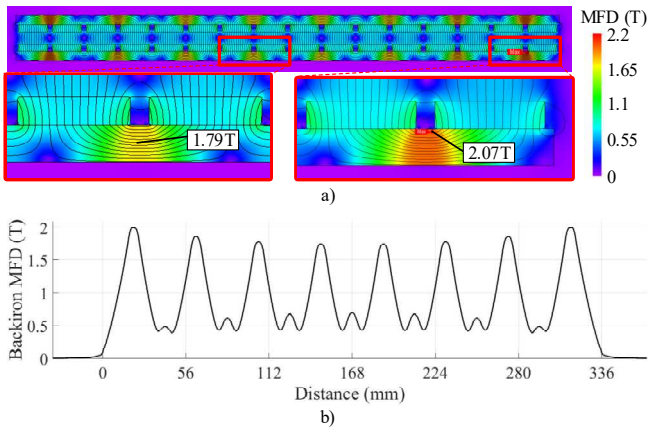

Fig.2 Magnetic field distribution in back iron of IL-PMLMs (a) MFD contour plot and flux line (b) MFD curve in back iron

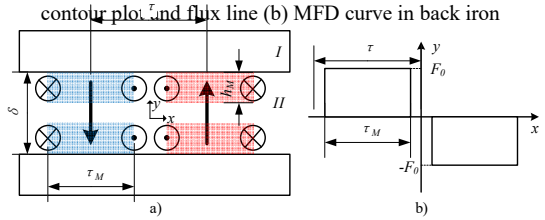

Fig.3 Model of U-type PMLM by Equivalent Magnetic Potential Method (a) Regions division (b) Distribution of equivalent magnetic potential

shown in Fig.2 (b). This means that thinning the back iron to achieve the goal of lightweight will cause magnetic saturation, which leads to a reduction in the air gap magnetic field.

This paper presents a novel method to reduce the peak MFD in back iron by using an end magnetic permeable block. The effectiveness of the method is verified by theoretical analysis and finite element calculation. Also, this paper provides a optimized parameter of the magnetic permeable block.

II. Basic Principle and Mathematical Model

By equating the excitation of the magnet to the magnetomotive force (MMF) generated by an infinitely thin coil, the model can be simplified into two regions: the air gap (II) and the back iron (I), which is shown in Fig.3 (a). Ignoring the magnetic flux leakage between the magnets, the equivalent MMF distribution can be expressed as Fig.3 (b) and Equ. (1)-(2).

$$\mathcal{F}(x)=\begin{cases}0 & k\tau-\frac{\tau-\tau_M}{2}\le x\le k\tau+\frac{\tau-\tau_M}{2}\\ (-1)^k F_0 & k\tau+\frac{\tau-\tau_M}{2}\le x\le k\tau+\frac{\tau+\tau_M}{2}\end{cases} \quad (1)$$

$$k=0,\pm1,\pm2,\dots$$

$$\mathcal{F}_0=\frac{B_r}{\mu_0}h_M \quad (2)$$

where, δ is the length of the air gap, τ is the pole pitch, τ_M is the width of the magnets, $\mathcal{F}_0$ is the MMF provided by magnets. B_r is the residual magnetism of magnets, h_M is the thickness of the magnets.

The equivalent magnetic circuit of the U-type PMLMs is shown in Fig.4. According to the principle of the nodal method, the magnetic circuit equations are list as (3).

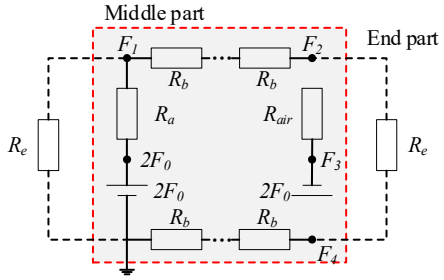

Fig.4 Equivalent magnetic circuit of U-type PMLMs

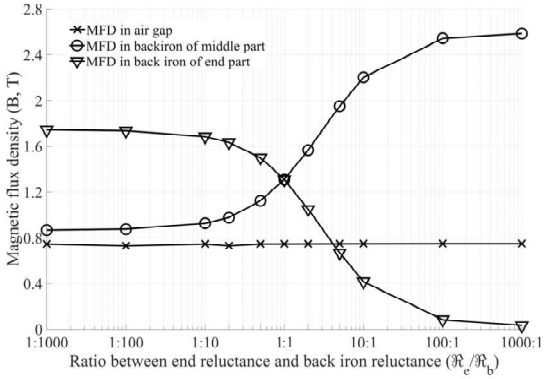

Fig.5 The influence of magnetoresistance ratio on magnetic flux density

$$\begin{bmatrix}\frac{1}{\mathcal{R}_a}+\frac{1}{\mathcal{R}_b}+\frac{1}{\mathcal{R}_e} & -\frac{1}{\mathcal{R}_b} & 0 & 0\\ -\frac{1}{\mathcal{R}_b} & \frac{1}{\mathcal{R}_a}+\frac{1}{\mathcal{R}_b}+\frac{1}{\mathcal{R}_e} & -\frac{1}{\mathcal{R}_a} & -\frac{1}{\mathcal{R}_e}\\ 0 & -\frac{1}{\mathcal{R}_a}-\frac{1}{\mathcal{R}_e} & \frac{1}{\mathcal{R}_e} & \frac{1}{\mathcal{R}_b}+\frac{1}{\mathcal{R}_e}\\ 0 & 0 & 1 & -1\end{bmatrix}\begin{bmatrix}\mathcal{F}_1\\ \mathcal{F}_2\\ \mathcal{F}_3\\ \mathcal{F}_4\end{bmatrix}=\begin{bmatrix}\frac{2}{\mathcal{R}_a}\mathcal{F}_0\\ 0\\ 0\\ -2\mathcal{F}_0\end{bmatrix} \quad (3)$$

where, $\mathcal{R}_a$, $\mathcal{R}_b$, $\mathcal{R}_e$ are air gap magnetoresistance, back iron magnetoresistance, and end magnetoresistance respectively, $\mathcal{F}_{1,2,3,4}$ are the magnetic potentials of nodes 1-4.

the magnetic flux flowing between two nodes can be expressed as (4).

$$\Phi_{mn}=\frac{\mathcal{F}_m-\mathcal{F}_n}{\mathcal{R}} \quad (4)$$

where, $\mathcal{F}_m$, $\mathcal{F}_n$ are the magnetic potentials of m and n nodes, respectively, $\mathcal{R}$ is the equivalent magnetoresistance.

The magnetic flux density is shown in (5) by assuming which is uniformly distributed in each region

$$B=\frac{\Phi}{S} \quad (5)$$

where, S is the cross-sectional area where magnetic flux passes.

Thus, through calculation, the influence of the ratio of the end magnetoresistance and the back iron magnetoresistance on the magnetic flux density in different parts of the U-type PMLMs be obtained as shown in Fig.5. It can be found that as the end magnetoresistance increasing, the MFD in the back iron increases, but the MFD in the end gradually decreases. Meanwhile, the MFD in the air gap is unaffected. When the end magnetoresistance is equal to the back iron magnetoresistance, the peak MFD in the soft magnetic material of the motor is the smallest.

Therefore, using the magnetic permeable block to shunt the side-end magnetic flux can realize the uniform interlinking of the magnetic fields between all magnets. Thus, the magnetic flux density in back iron can also be reduced to relieve back

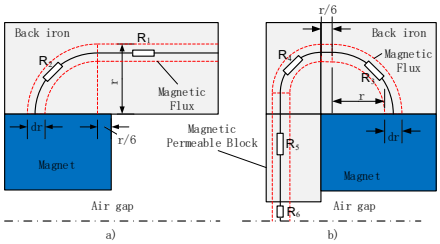

Fig.6 Refined model of magnetoresistance at different positions in the U-type PMLM (a) Middle part (b) End part

iron saturation.

III. Optimization of Magnetic Permeable Block

The refined magnetoresistance models of the back iron and the end magnetic permeable block are shown in Fig.6. For the back iron in the middle part of the U-type PMLMs, the partial magnetic circuit is shown in Fig.6 (a). The magnetoresistance of this part can be expressed by (6) – (8).

$$\mathcal{R}_b = \mathcal{R}_1 + \mathcal{R}_2 \tag{6}$$

$$\mathcal{R}_1 = \frac{\mu_0 \mu_r \tau (1-\alpha_p)}{2 \Delta_1 l_M} \tag{7}$$

$$\mathcal{R}_2 = 2\left(\int_0^{\Delta_1} \frac{\mu_0 \mu_r l_M}{\left(\frac{\pi}{2}+\frac{1}{6}\right) r} dr \right)^{-1} \tag{8}$$

where, α_p is the polar arc coefficient, Δ_1 is the thickness of the back iron, l_M is the height of the magnets.

For the ends of U-type PMLMs, the partial magnetic circuit is shown in Fig.6 (b). And the magnetoresistance of this part can be expressed by (9) – (13).

$$\mathcal{R}_e = \mathcal{R}_3 + \mathcal{R}_4 + \mathcal{R}_5 + \mathcal{R}_6 \tag{9}$$

$$\mathcal{R}_3 = \left(\int_0^{\Delta_1} \frac{\mu_0 \mu_r l_M}{\left(\frac{\pi}{2}+\frac{1}{6}\right) r} dr \right)^{-1} \tag{10}$$

$$\mathcal{R}_4 = \left(\int_0^{\Delta_2} \frac{\mu_0 \mu_r l_M}{\left(\frac{\pi}{2}+\frac{\Delta_1}{\Delta_2}-1\right) r} dr \right)^{-1} \tag{11}$$

$$\mathcal{R}_5 = \frac{\mu_0 \mu_r (\Delta_2 - \Delta_1)}{\Delta_2 l_M} \tag{12}$$

$$\mathcal{R}_6 = \frac{\mu_0 (\delta + h_M + \Delta_1 - \Delta_3)}{\Delta_2 l_M} \tag{13}$$

where, Δ_2 and Δ_3 are the width and length of the magnetic permeable block, δ is the air gap length.

According to the derivation in subsection II, when $\mathcal{R}_b$ is closer to $\mathcal{R}_e$, the peak magnetic flux density in the back iron is better. Therefore, the optimization problem for size parameters is shown in (14).

TABLE I
MAIN PARAMETERS OF FEA MODELS

Parameter	Description	Value
τ	Pole distance	21 mm
Δ_1	Back iron thickness	6 mm
h_M	Magnet thickness	5 mm
δ	Air gap width	7.5 mm
α_p	Pole-arc coefficient	0.667
τ_M	Magnet width	14 mm
l_M	Magnet length	75 mm
p	Pole pairs number of unit motor	4
	Back iron material	#10 steel
	Magnet grade	N38H

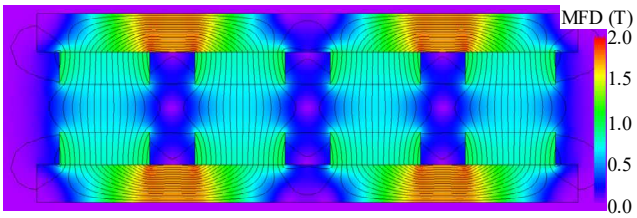

Fig.7 Magnetic field distribution of traditional U-type PMLMs

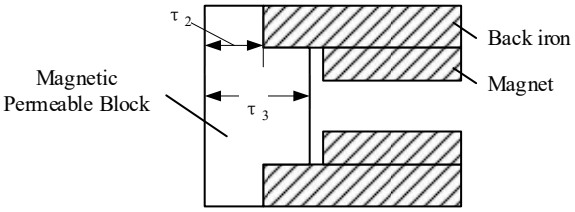

Fig.8 Structure of magnetic permeable block

$$\begin{aligned} min\ & \Delta\mathcal{R} = |\mathcal{R}_b - \mathcal{R}_e| \\ s.t.\ & \Delta_2 \geq 0 \\ & \Delta_3 \geq 0 \end{aligned} \tag{14}$$

IV. Finite Element Analysis

A finite element analysis model of U-type PMLM is established to verify the above inference, whose main parameters are shown in TABLE I. And the magnetic field distribution is shown in Fig.7.

Aiming at the above U-type PMLM, the optimized size of the end magnetic permeable block processed by DT4E is $\Delta_2 = 9$ mm and $\Delta_3 = 14.75$ mm. Therefore, the end magnetic permeable block structure as shown in Fig.8 can be used, where, τ_2 is 6mm and τ_3 is 9mm. The magnetic flux density contour plot of U-type PMLM with the end magnetic permeable block is shown in Fig.9.

Comparing with Fig.7 and Fig.9, it can be found that the magnetic flux density in back iron can be significantly reduced by using an end magnetic permeable block. The magnetic flux density curve in the back iron is shown in

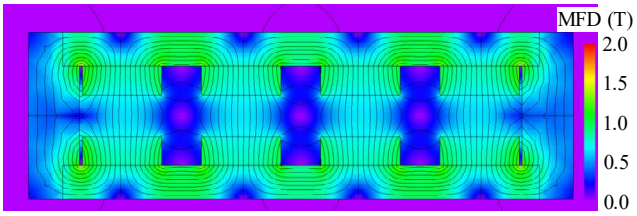

Fig.9. Magnetic field distribution of U-type PMLMs with end magnetic permeable block

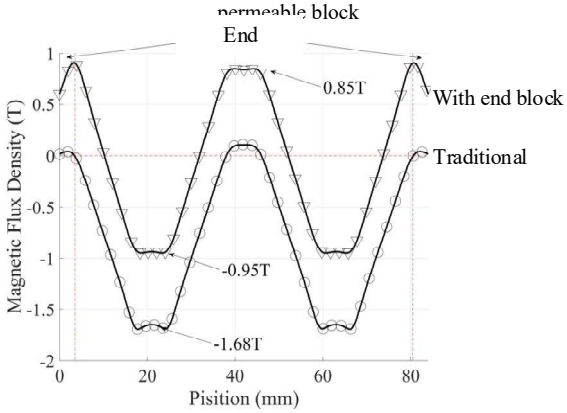

Fig.10 Magnetic flux density curve in back iron

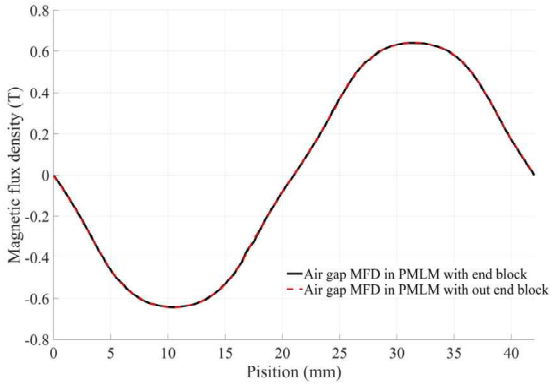

Fig.11 Magnetic flux density curve in air gap

Fig.10. And it can be found that the peak magnetic flux density in the back iron dropped from 1.68T to 0.95T by using a magnetic permeable block.

The distribution of the air gap magnetic flux density in the FEA result is shown in Fig.11. It can be seen that the air-gap flux density of the U-shaped motor is the same regardless of whether there is an end magnetic permeable block or not. So it can be inferred that the end magnetic permeable block will not affect the output characteristics of the linear motor. Therefore, installing the magnetic permeable block at the end of the U-type PMLMs can reduce the magnetic saturation in the back iron by reduce the peak magnetic density in the back iron effectively.

V. Conclusion

A novel method for optimizing the magnetic field in the back iron is proposed in this paper. And the FEA result shows that the peak magnetic flux density in the back iron can be reduced by 43% by employing the appropriate size of the magnetic permeable block at the end of U-type PMLMs without affecting on air gap magnetic flux density.

References

[1] L. Lei, Y. Haitao, F. Teng, and D. Kun, "Design and Analysis of a Linear Oscillatory Motor with Moving Magnet," *Micromotors,* 2017.

[2] H. Lu, J. Zhu, and Y. Guo, "A permanent magnet linear motor for micro robots," in *2005 International Conference on Power Electronics and Drives Systems*, 2005, vol. 1: IEEE, pp. 590-595.

[3] N. Sang *et al.*, "A Dual-Sided Hybrid Excitation Eddy Current Damper for Vibration Suppression in Low Damping Linear Motor System," *IEEE Transactions on Industrial Electronics,* 2020.

[4] L. Ki-Chae, W. Joon-Keun, K. Gyu-Hong, H. Jung-Pyo, and K. Gyu-Tak, "Detent force minimization techniques in permanent magnet linear synchronous motors," *IEEE Transactions on Magnetics,* vol. 38, no. 2, pp. 1157-1160, 2002, doi: 10.1109/20.996296.

[5] L. Li, D. Pan, and X. Huang, "Analysis and Optimization of Ironless Permanent-Magnet Linear Motor for Improving Thrust," *IEEE Transactions on Plasma Science,* vol. 41, no. 5, pp. 1188-1192, 2013, doi: 10.1109/TPS.2013.2245425.

[6] P. Sun and H. Zhou, "Air-gap magnetic field design optimization for U-shaped ironless permanent magnet linear synchronous motors," in *2008 International Conference on Electrical Machines and Systems*, 2008: IEEE, pp. 358-363.

[7] Q. Shuheng, Z. Jie, and Z. Chi, "Effects of Halbach and Non-Halbach Arrays on Thrust Characteristics of Ironless Permanent Magnet Linear Motors: A Simulation and Optimization," in *2020 23rd International Conference on Electrical Machines and Systems (ICEMS)*, 24-27 Nov. 2020 2020, pp. 1659-1662, doi: 10.23919/ICEMS50442.2020.9291096.

[8] L. Zhang, B. Kou, F. Xing, and B. Zhao, "Characteristic analysis of an ironless linear synchronous motor with novel halbach magnet array," in *2014 17th International Symposium on Electromagnetic Launch Technology*, 7-11 July 2014 2014, pp. 1-5, doi: 10.1109/EML.2014.6920212.

[9] L. Zheng, Z. Jiazhen, Z. Ruodong, and W. Qunjing, "No-load Magnetic Field Analysis of the U-shaped Ironless Permanent Magnet Synchronous Linear Motor," *Recent Advances in Electrical & Electronic Engineering (Formerly Recent Patents on Electrical & Electronic Engineering),* vol. 11, no. 1, pp. 26-32, 2018.